

Accepted Manuscript

A Combination of GFRP Sheets and Steel Cage for Seismic Strengthening of Shear-Deficient Corner RC Beam-Column Joints

Esmael Esmaeeli, Fakhreddin Danesh, Kong Fah Tee, Sassan Eshghi

PII: S0263-8223(16)30839-X

DOI: <http://dx.doi.org/10.1016/j.compstruct.2016.09.064>

Reference: COST 7790

To appear in: *Composite Structures*

Received Date: 6 June 2016

Revised Date: 9 August 2016

Accepted Date: 22 September 2016

Please cite this article as: Esmaeeli, E., Danesh, F., Tee, K.F., Eshghi, S., A Combination of GFRP Sheets and Steel Cage for Seismic Strengthening of Shear-Deficient Corner RC Beam-Column Joints, *Composite Structures* (2016), doi: <http://dx.doi.org/10.1016/j.compstruct.2016.09.064>

This is a PDF file of an unedited manuscript that has been accepted for publication. As a service to our customers we are providing this early version of the manuscript. The manuscript will undergo copyediting, typesetting, and review of the resulting proof before it is published in its final form. Please note that during the production process errors may be discovered which could affect the content, and all legal disclaimers that apply to the journal pertain.



A Combination of GFRP Sheets and Steel Cage for Seismic Strengthening of Shear-Deficient Corner RC Beam-Column Joints

Esmael Esmaeli¹, Fakhreddin Danesh², Kong Fah Tee¹, Sassan Eshghi³

¹ Department of Engineering Science, University of Greenwich, UK

² Faculty of Civil Engineering, K. N. Toosi University of Technology, Iran

³ International Institute of Earthquake Engineering and Seismology (IIEES), Iran

ABSTRACT

This paper is focused on the performance of a proposed scheme for seismic strengthening of shear deficient joints of 3D reinforced concrete (RC) corner beam-column connections. This technique is composed of a combination of GFRP sheets and a steel cage, and does not require perforating the existing concrete elements to anchor the FRP sheets. Two similar full-scale beam-column connections were made without any transverse reinforcement in their joint region. One of which was tested in its as-built condition, taken as control specimen, while the other one was tested after strengthening. Seismic behaviour of these specimens were studied under a cyclic loading pattern imposed simultaneously with a constant column's axial load. Comparison of the test results of these specimens revealed a noticeable improvement in the seismic response of the strengthened specimen. This achievement along with the application feasibility of this technique indicates the suitability of the proposed strengthening scheme for practical applications. Finally, the experimentally obtained joint shear strength of the control and retrofitted specimens are compared to the one estimated by the relationships of the softened strut-and-tie model and ACI-318, respectively. This comparison revealed a satisfactory prediction of joint shear strength for both specimens, the as-built and the strengthened one.

KEYWORDS

Seismic retrofitting; RC beam-column joint; GFRP sheets; Steel cage; Bidirectional loading, Cyclic behaviour; Anchorage system

1. INTRODUCTION

Insufficiency or lack of transverse shear reinforcement in the joint region of beam-column connections of RC structures subjected to earthquake, e.g. those designed only for gravity loads or with constructional deficiencies in spite of adequate seismic design practice, may result in brittle shear failure of the joint. Even if the adjoining members are designed following strong column-weak beam requirements, this kind of premature failure prevents the development of plastic hinge at the ends of the beams and causes instability in gravity load carrying capacity of the corresponding column. Hierarchy of this type of failure jeopardizes the safety performance of the structure subjected to the lateral loading to an extent that a catastrophic collapse of the building may occur.

The rehabilitation of such seismically deficient structures has received much attention during the last decades [1, 2]. Application of Fibre Reinforced Polymers (FRPs) is the most common proposed strengthening solution [3-11]. However, as reported by several researchers [12-15], premature FRP debonding often adversely affects the efficiency of the strengthening scheme and prevents utilizing the full capacity of the FRP material. Hence, further investigations on application of FRPs for seismic rehabilitation of deficient joints have been oriented mainly toward the use of mechanical anchorages to prevent/delay debonding failure [4, 13, 14, 16-19]. The importance of using appropriate anchorages for FRP retrofitted joints is well highlighted in the experimental investigation conducted by Ghobarah and Said [13]. Different strengthening schemes based on wrapping exterior simplified two-dimensional joints by Glass-FRP (GFRP) were examined by these authors, aiming to prevent the joint shear failure mode. While premature debonding of GFRP strengthened joint without mechanical anchorage resulted in joint shear failure, the GFRP strengthened specimens with their edges anchored by means of steel plates fastening system developed a flexural plastic hinge at their beam's end. Parvin et al. [18] used CFRP sheets and wraps along with CFRP strips anchored into the perforated holes on the beam, for the seismic strengthening of two-dimensional exterior joints. Debonding of U-shaped CFRP

layers extended and bonded on the lateral face of the beams and the rupture of FRP strip, used as the anchorage system, were reported.

Installing and anchoring FRP sheets for strengthening of 3D beam-column connections is a challenge, since it is practically difficult to ensure an effective wrapping at the joint region. Due to the existence of orthogonal beams, three- or four-side wrapping of the joint region is not possible. Extending and anchoring the composite layers on the lateral faces of the beams may increase the flexural capacity of them, which may prevent the formation of the plastic hinge at the end of these beams while increases the shear demand at the joint region. The existence of the floor slab makes the anchoring task of FRP sheets even more complicated. Moreover, installing the metallic anchorage systems may cause stress concentration in the FRP and promote its premature rupture. Esmaeeli [20] recently proposed a combination of strain hardening cementitious composite (SHCC) and FRP sheets/laminates in the form of cast-in-place solution or a prefabricated plate (Hybrid Composite Plate-HCP) for the retrofitting of RC structures. HCP can be attached to the substrate using mechanical anchors, since SHCC offers sufficient bearing capacity [21]. Both solutions, cast-in-place and HCP, showed noticeable improvements in the seismic performance of repaired severely damaged two-dimensional interior RC beam column joints [22,23].

To achieve enough bond development length for the anchorage systems made of bonded FRP strips, their full wrapping around the beam is necessary. However, this requires perforation on the floor slab, which is a destructive task and consumes noticeable time and labour work.

In the current study, a novel strengthening technique using bidirectional GFRP layers and a steel cage is proposed. Using this strengthening technique, the enhancement in the seismic performance of a 3D RC corner beam-column joint, especially increasing its joint shear strength, is attempted. The corner beam-column joint is selected in this study due to its higher vulnerability than other types of joints when subjected to a lateral loading. A corner joint has only two orthogonal adjoining beams which is not sufficient for efficient joint confinement, and its adjoining columns carry an imbalanced bending moment. The practical difficulties of applying FRP

sheets to this joint, which is caused by the existence of the orthogonal beams, is facilitated through anchoring the GFRP layers to the steel cages placed around the column. This arrangement does not require any perforation on the structure to be retrofitted.

2. EXPERIMENTAL PROGRAM

2.1. Test specimens

Two similar full-scale 3D RC corner beam-column connections, without any transverse reinforcement in their joint region, were prepared and tested under a cyclic load history discussed in section 2.3. The one designated TS was taken as the reference specimen, thus tested in its as-built condition. The other specimen, designated TSR, was tested after it was retrofitted adopting a proposed scheme detailed in section 2.4.

Each specimen was composed of an upper and a lower column along with two orthogonal beams, all coinciding in the joint region. The length of the elements was representative of the mid-height and mid-span of beams and columns of a real structure, respectively. This configuration was adopted to facilitate the simulation of the boundary conditions at the extremity of the elements in the laboratory, as the contra-flexure points of a moment-sway frame subjected to lateral loading approximately occur at the mid-length of its beams and columns.

Fig. 1 represents the geometry of the specimens and the details of their longitudinal and transverse reinforcements. Longitudinal steel bars of the beams and columns were designed to satisfy the weak beam-strong column requirement of ACI 318-14 [24]. Following the recommendations of ACI-ASCE Committee 352 [25], beams' longitudinal bars were anchored at the joint region using standard 90° hook configuration. However, due to the limitation in the depth of the columns the development length of these anchors, l_{dh} , was 70 mm shorter than the length recommended by equation 18.8.5.1 of ACI 318-14 [24]. Moreover, to produce large enough shear stresses in the joint, beam depth-to-bar diameter ratio, recommended by ACI 352R-02 [25], was neglected. To assure that failure occurs in the joint of the as-built specimen, shear reinforcements were placed closely-spaced along the length of the beams and the columns (see Fig. 1).

2.2. Test setup

The adopted test setup is illustrated in Fig. 2. Due to the laboratory limitations, the beam-column joint was tested with the horizontally placed column. As depicted in Fig. 3, 4 mm thick steel plates were bonded to the lateral faces of each column at their supported end. Using another set of steel plates, each of 15 mm thickness, an exterior gapless box around the thinner plates was arranged. The contact surfaces between the exterior and interior jackets were lubricated to assure their relative sliding with a minimized friction. Close to the extremity of each column, a steel frame was secured to the strong floor of the laboratory, perpendicular to the column's longitudinal axis, to support specimen's lateral reactions. As depicted in Fig. 2 and Fig. 3, four identically designed mechanical hinges were placed at the supported-ends of each column to release rotations in both vertical and horizontal planes of the test setup (bidirectional free-rotation). Each mechanical hinge was composed of a fixed and a rotatable part. The fixed part was attached to the supporting frame, while the rotatable one was connected to the exterior steel box.

There was a reaction frame, secured to the strong floor of the laboratory, close to the end of each column and oriented along the columns' longitudinal axis. Column axial load was imposed by means of a hydraulic jack which was fixed to the end of one of the columns at its stroke-end and to the supporting reaction frame at the other end. Similarly, a load-cell was installed at the end of the other column to measure the axial reaction of the column and to transfer it to the supporting frame.

A servo-control hydraulic actuator was installed at the free-end of each beam to apply cyclic quasi-static loading. As shown in Fig. 2, these actuators were supported by the reaction steel elements secured to the ground floor.

2.3. Loading history

The loading pattern was composed of simultaneous column constant axial load of 370 kN, corresponding to approximately 10% of the nominal axial capacity of the column, and quasi-static

reversed cyclic loading imposed to the free ends of the orthogonal beams. The cyclic load pattern, partially depicted in Fig. 4, included both unidirectional and bidirectional cycles. This loading history was controlled using drift-angle, defined as the percentage of the displacement at the loaded-end of the beam to the length between the loaded-end of the beam and the centre-line of the column. The plane of the vertically placed beam, designated vertical plane hereafter, was taken as the main loading direction. Initially two cycles of 0.4% drift-angles were imposed on the vertical beam to verify the performance of the instrumentation. Afterward, one cycle of 0.6% was imposed to each of vertical and horizontal beams, sequentially. The next two cycles, with 0.8% drift-angle, were introduced to the vertical beam. At this point, to simulate the bidirectional loading, load cycles were also imposed on the horizontally placed beam, hereafter designated horizontal plane, at the intervals represented in Fig. 4. In all bidirectional loading cycles, the vertical beam was initially pushed up to its target drift-angle and while it was kept at this position, the other beam was moved to the same drift-angle. Afterward, the vertical beam was unloaded to return to its original position and while remained in this location, the horizontal beam was unloaded in a similar manner. This loading process was continued at the remained half cycle, but to the opposite direction (pull direction), to complete the bidirectional cycles. Similarly to the unidirectional cycles, at each pre-defined drift-angle, bidirectional cycles were also repeated two times. Two different combinations of bidirectional loadings were introduced to simulate the most critical loading condition; bidirectional loadings without phase difference (both beams moved to the same direction) and those with 180° of phase difference (beams displaced to the opposite directions). Set of loadings enclosed in the dashed-line rectangle in Fig. 4 were repeated by increasing 0.8% their drift-angle (the drift-angle of the next set of loadings, imposed immediately after those enclosed in the dashed-rectangle, were 1.6% and 2.0%, sequentially). The next series of the cycles followed the explained load protocol. The test was terminated when the loss in the maximum storey shear in the vertical plane exceeds 30%.

2.4. Rehabilitation scheme

The proposed seismic strengthening scheme is composed of bonding the GFRP sheets, on the joint region and part of the columns at the vicinity of the joint, and then anchoring the free edges of these composite layers to a metallic cage. The metallic cage, made of angle steel profiles, was placed at each corner of the column along the GFRP wraps.

The wet layup composite system was made of bidirectional glass fabric impregnated in an epoxy resin. The orthogonal fibres of the bidirectional GFRP sheet were oriented along the beam and the columns longitudinal axes in each of the vertical and the horizontal plane of the specimen.

The layout of the four layers of glass fabric used for the strengthening of the specimen TSR is shown in Fig. 5. The number of GFRP layers was determined based on a previously performed finite element study [8]. As illustrated in Fig. 5, the fabric was cut partially along the positions of the bottom and top faces of the beams. As notified in the legend of this figure, the extensions of the cuts are shown by the thick lines.

Fig. 6 schematically illustrates the strengthening scheme applied to the TSR. The upper and lower regions of the composite layers, 350 mm each as shown in Fig. 5, were fully wrapped around the columns, with 100 mm of overlap. The middle-portion of the composite, 300 mm, was bonded on the free faces of the joint. However, the extensions of the composite on the lateral faces of the beams were kept un-bonded.

Each angle steel profile (L80 = 80mm × 80mm × 8 mm), showed in Fig. 6, was placed at its corresponding corner on the columns (note the numbering of the corners of the columns). To each of these L80 profile, smaller angle steel profiles were welded (L40 = 40mm × 40 mm × 4 mm).

A 12 mm diameter hole was drilled on the centre of the free leg of each L40 steel angle in order to pass the threaded rods and to tie L80 profiles to each other. To prevent the stress concentration in the GFRP at the corners of the column, thin rubbers were placed along the interfaces of L80 profiles and the GFRP. Moreover, corners of the columns at the strengthened regions were rounded to a radius of 15 mm and then smoothed to avoid stress concentrations in the GFRP

system and to prevent accumulation of the air voids beneath these strengthening layers. Because of the existence of the beams, one leg at the central portion of angle profiles which were designed to be installed at column corners number 1 and 3, as labelled in Fig. 6, was cut in a length equal to the depth of the beams (see detail “C” in Fig. 6). Moreover, three 12 mm diameter threaded-holes were drilled on the remained leg of each of these profiles. Steel profiles were tied to each other by means of 10 mm diameter threaded-rods and nuts, applying a torque of 10 N.m. Afterward, each of the un-bonded portions of the GFRP sheets was folded back over the steel profile and anchored on it by means of a thin steel plate and three 12 mm diameter short bolts, without perforation in concrete (see both the side view and the detail “B” in Fig. 6).

It should be noted that to prevent stress concentration at the GFRP layers due to the sharp cut-edge of the steel profiles at the corners 1 and 3 of the columns, a 14 mm diameter plain steel bar was welded to this edge of each of these profiles (see detail “C” in Fig. 6). The entire process of the installation of the steel profiles and anchoring GFRP was performed during the allowed working time of the epoxy resin.

2.5. Material Properties

Two ready-mix batches of concrete were used to cast the specimens. The average nominal compressive strengths of three standard concrete cylinders (150 mm × 300 mm) for specimens TS and TSR on the test day were 28.7 MPa and 31.2 MPa, respectively. The average yield strength of longitudinal and transverse bars was 498 and 365 MPa, respectively. The average mechanical properties of the used bidirectional glass fabric and the epoxy resin are given in Tables 1 and 2, respectively, based on the supplier’s specifications. The nominal tensile strength of the impregnated strand of the glass fibres is 2400 MPa and the nominal tensile force per meter of composite width in each direction, for the design based on the fabric thickness, is 160.8 kN/m.

2.6. Instrumentation

To measure the strains in the reinforcing bars of each beam-column joint, twenty-four strain gauges were bonded at the different locations on these bars. Moreover, seven strain gauges were

bonded to different locations on the GFRP sheet. Two linear variable differential transducers (LVDTs) were placed diagonally at the joint region in the vertical plane. Using the results of these LVDTs, the shear distortion of the joint was calculated. Shear forces in the beams were measured by the load cells installed on the hydraulic actuators. The axial reaction of the column was registered by means of a load-cell installed at its end. Detailed information about instrumentations of specimens and their results can be found in [26].

3. OVERALL RESPONSE OF THE SPECIMENS

In this section, the overall behaviour of the specimens is described by means of their hysteretic behaviour, crack pattern and failure mode.

3.1. Specimen TS

Hysteretic curves of storey-shear *versus* drift-angle in both vertical and horizontal planes of the reference specimen, TS, are shown in Fig. 7. According to these figures, this specimen reached its maximum storey-shear capacity at 1.6% drift-angle in both push and pull loading directions with their corresponding shear capacities reported in Table 3. As illustrated in Fig. 8, except for few flexural cracks, formed on the beams close to the joint region, the majority of damages were concentrated on the joint and columns at the vicinity of the joint region. Due to the joint shear deficiency, inclined cracks in the joint region caused rapid degradation in storey-shear capacity. None of the reinforcements of the beams or columns yielded.

Introducing further cycles with higher amplitude, beyond the peak load, only increased the width of the existing cracks. The crushing and spalling of concrete at the joint region was also observed close to the termination of the test.

3.2. Specimen TSR

Fig. 9 represents curves of the hysteretic storey-shear *versus* drift-angle in both vertical and horizontal planes of the strengthened specimen, TSR. The longitudinal bars of both beams, in both opposite faces, were yielded in the cycles corresponding to the maximum storey-shear ca-

capacity in each loading plane, before reaching the peak load. The values of the storey-shear and the drift-angle corresponding to the yield of these steel bars are indicated in Table 4. Yielding of the longitudinal reinforcement of the beams resulted in the formation of a plastic hinge, concentrated at the interface between each beam and the joint.

The strengthened specimen experienced its maximum storey-shear capacity in the vertical plane at drift-angle of 2.0% for both push and pull directions. The corresponding shear capacities in horizontal plane occurred at drift-angles of 2.4% and 2.0%, respectively. The storey-shear capacities of the specimen TSR are indicated in Table 5. The peak load dropped more than 30% at 6% drift-angle in vertical plane and the test was terminated.

According to the status of damages at the end of the test of this specimen, presented in Fig. 10(a), the flexural cracks distributed along the length of both beams and the GFRP composite was undamaged. After the test, to examine the state of the concrete at the joint region beneath the strengthening scheme, the steel cage was partially released and the composite layer in this region was cut and detached, see Fig. 10(b). This inspection revealed that the concrete at the joint was uniformly crushed rather than having macro-cracks. As mentioned before, a wide flexural crack was formed at the interface of each beam and the joint, where the beams longitudinal bars were yielded (e.g. this crack in the vertical plane is shown in Fig. 10(b)). The efficient concrete confinement at the joint prevented penetrating of this crack into the joint region and also merging the micro-cracks at the joint region into the macro ones. The uniformly crushed concrete in the entire joint region and the wide flexural crack of the beams adjacent to the joint indicate the effectiveness of the proposed strengthening scheme in confining the joint's concrete. This confinement has increased the joint shear strength and maintained its integrity up to the large drift-angles.

4. COMPARISON AND DISCUSSION OF THE TEST RESULTS

In this section, the response envelopes, displacement ductility, stiffness, contribution of shear deformation of the joint in the storey-drift, cumulative dissipated energy, bi-directional joint

shear interaction, and the joint shear strength of both specimens are discussed and compared to each other. The above mentioned parameters are examined in the vertical plane.

Response envelope: envelope curve of the hysteresis loops of storey-shear *versus* drift-angle for both control and strengthened specimens are shown in Fig. 11. The proposed strengthening technique resulted in 60% average increase in the storey-shear capacity of specimen TSR (average value of push and pull loading directions), as compared to the reference specimen, TS. Moreover, the average drift-angle at the peak loads (push and pull loading directions) of TSR is 25% higher than the corresponding value of TS.

Displacement ductility: structural elements subjected to reversal cyclic loadings, such as seismic action, are expected to undergo large deformation without significant loss in their ultimate load carrying capacity. This characteristic along with sufficient energy dissipation capacity are the fundamental requirements for the reasonable and economic design of the structures subjected to earthquake loading. Comparison of the post-peak response in envelope curves of TS and TSR, presented in Fig. 11, reveals a significant enhancement in ductility performance of the strengthened specimen. According to this Figure, the rapid degradation in post-peak strength of the reference specimen, occurred in both push and pull loading directions, turned into an almost plateau regime in the case of the strengthened specimen with only an initial negligible drop in its maximum storey-shear capacity which is less than 9%. Up to an average drift-angle of 3.6%, for push and pull loading directions, this post-peak strength was remained almost constant. However, beyond this point the rate of the strength degradation, due to the sliding of the longitudinal rebars of the beams, has increased. Adopting a balanced energy approach discussed in [23], the equivalent bilinear perfectly elastoplastic curves of the storey-shear *versus* drift-angles for both specimens were determined. Using the obtained bilinear curve, the displacement ductility factor for each specimen was calculated as the ratio of the ultimate displacement to the yield displacement. The displacement corresponding to 15% drop in the maximum storey-shear capacity was taken as the ultimate displacement. According to this definition, the ultimate dis-

placement of TS and TSR is 30 mm (drift-angle of 2.0%) and 72 mm (drift-angle of 4.8%), respectively. Following this method, the average displacement ductility factors (the average value of push and pull loading directions) of 1.96 and 2.5 were obtained for TS and TSR, respectively. Therefore, the proposed strengthening scheme provided TSR with 28% higher displacement ductility than TS.

Joint shear deformation: using the data registered by the diagonal LVDTs, installed on the joint of each specimen, the shear distortion of the joint at each loading step was obtained. Furthermore, the contribution of the joint shear deformation to the drift-angle for each specimen was calculated and presented in Fig. 12. According to this figure, while at 2.4% drift-angle, this contribution for the control specimen is 54%, the corresponding value for the strengthened specimen is only about 20%. The flat region of the contribution of joint shear deformation of specimen TSR in this figure, between 2% and 4% drift-angles, is associated with flexural deformation at the beam's plastic hinge. The sudden increase in the contribution of joint shear deformation of this specimen, beyond drift-angle of 4% is attributed to the rapid degradation in shear stiffness of the joint and also to the sliding of beam's longitudinal bars.

Stiffness: the slope of the line connecting the peak-loads at push and pull loading directions of a cycle, is taken as the secant stiffness. Following this definition, for both specimens, the secant stiffness at the first cycle of the unidirectional loading cycles with equal amplitude is calculated and depicted in Fig. 13. As shown in this figure, the initial stiffness, stiffness calculated at 0.4% drift-angle, of the rehabilitated specimen is about 14% higher than the control one. This increase is mainly associated with the use of the steel cage as part of the strengthening solution. The steel cage reduced rotation of the columns at the vicinity of the joint. As it is evident by Fig. 13, up to 0.6% drift-angle there is only a marginal difference in the stiffness of the specimens. Beyond this drift-angle, however, the strengthened specimen, TSR, presents a noticeably higher stiffness as compared to that of the reference specimen, TS. At the ultimate displacement of TS, drift-angle of 2.0% corresponding to approximately 15% maximum load drop, the secant stiffness of

the strengthened specimen is 1.4 times higher than the corresponding one of the reference specimen.

Cumulative dissipated energy: high energy dissipation capacity is a desirable characteristic for the structures expected to endure severe earthquake reversal cycles without significant loss in their functional performance. The area enclosed in a hysteresis loop at a given cycle represents the energy dissipated by the specimen during that cycle. For each specimen, the cumulative dissipated energy *versus* time and drift-angle is plotted in Fig. 14, up to their ultimate displacement. At this ultimate point, the dissipated energy in specimen TSR is 10.7 times higher than that of the specimen TS. This achievement reflects the notable efficiency of the proposed strengthening scheme in enhancing energy dissipation capacity, which means strengthened specimen withstands a more severe seismic action as compared to its as-built condition.

Bidirectional loading interaction: bidirectional loading resulted in the vertical segments in hysteretic responses of the specimens (Figures 7 and 8), indicating reduction in the storey-shear strength. Fig. 15 represents interaction orbits at the first bidirectional cycle of 0.8% and 1.6% drift-angles (zero phase difference) for both specimens, while Fig. 16 depicts the corresponding orbits at the first bidirectional cycle of 1.2% and 2.0% drift-angles (180° phase difference). In each figure, beams' displacement orbits and storey-shear orbits are presented at the left and right hand sides, respectively. The loading sequences are identified with the arrows. The arrow with a dot-shape at its beginning distinguishes the first loading ramp. From the displacement orbits it can be seen that displacing the horizontal beam caused an initial increase in the displacement of the vertical-beam (for example see points "a", "b" and "c" also points "d", "e" and "f" in displacement orbits of Fig. 15). This increase was accompanied with an increase in the shear-storey at the vertical plane, but once the displacement of the vertical beam is stabilized the corresponding storey-shear started to decrease (for example see points "a'", "b'" and "c'" also points "d'", "e'" and "f'" in the storey-shear orbits of Fig. 15). Skewed-shape of the storey shear orbits indicates the reduction in the shear-capacity of the joint due to the bidirectional loading

effect. Comparison of the storey-shear orbits of the specimen TSR with the ones of the specimen TS, in Figures 15 and 16, specifies that the strengthened specimen is less affected by the bidirectional loading, as its orbits are less skewed compared to the ones of the TS.

To quantify this effect, the percentage of reduction in storey-shear in the vertical plane due to the loading in the orthogonal direction is calculated and reported in Table 6 and Table 7, for bidirectional loadings without and with phase difference, respectively. For the purpose of this calculation, once the horizontal beam reached its target drift-angle, the storey-shear in the vertical plane is compared to its maximum storey-shear during this ramp of loading on the horizontal beam (for example storey-shear at the vertical plane at point “b” and “c” or “e” and “f” in Fig. 15 were compared to each other). The average values of storey-shear reduction in Table 6 and Table 7, average of positive and negative loading directions, indicate that such reduction in specimen TS is 1.6 to 2.8 times larger than the reduction occurred in TSR. Moreover, no meaningful difference in the reduction of storey-shear due to the type of bidirectional loading, loadings with and without phase difference, can be observed.

Joint shear strength: from the stress equilibrium at the free body of the joint, the horizontal shear force in a corner joint, V_{jh} , can be obtained as:

$$V_{jh} = T_{sh} - V_{col} \quad (1)$$

where T_{sh} is the tensile force in the longitudinal bars of the beam at the interface with the joint, and V_{col} is the horizontal column shear just above the joint. The tensile force in the longitudinal bars of the vertical beam, T_{sh} , is calculated using the strain values, ϵ_{st} , registered by the strain gauges bonded to these bar at the vicinity of interface of the beam and the joint. For both specimens, the tensile strains in longitudinal reinforcements of the vertical beam at the section close to the joint versus the drift-angle, up to the peak load, are presented in Fig. 17. The shear strength of each specimen, calculated using Equation 1, along with the parameters used for these calculations are reported in Table 8. According to this table, the average of horizontal joint shear strength, V_{jh}^{exp} , in the vertical plane of specimen TS and specimen TSR is 390 kN and 573

kN, respectively. Therefore, the proposed strengthening scheme provided the joint with 47% shear strength increase as compared to its as-built maximum shear capacity.

5. PREDICTION OF THE JOINT SHEAR STRENGTH

There is not yet a consensus among the researchers in regards to the mechanism of shear transfer in a joint which is part of a beam-column connection subjected to the large lateral reversal deformations. Perhaps the diagonal strut and the truss mechanisms are the most rational shear transfer model [27]. However, the contribution of the truss mechanism depends on the bond quality between rebars and the concrete in the joint region. It is speculated that in most cases the reversals of the loads significantly deteriorate this bond strength, thus at the ultimate state the shear stresses are only resisted by the diagonal strut. Cracking in the joint region adversely affects the compressive strength of the diagonal strut, which is known as the softening effect due transverse cracking. If the cracked diagonal strut is considered as the only shear resisting mechanism, the horizontal joint shear strength can be estimated using the relationship proposed by Hwang et al. [28] in their simplified softened strut-and-tie (SST) model, as represented below:

$$V_{jh}^{SST} = \xi f'_c A_{str} \cos \theta \quad (2)$$

where θ is the angle of inclination between diagonal strut and the horizontal axis; ξ is the softening coefficient approximated by $3.35/\sqrt{f'_c} \leq 0.52$ [29]; and $A_{str} = a_s \times b_s$ is the effective section area of diagonal strut. The width of the diagonal strut, b_s , can be taken as the effective width of the joint, following the recommendations of ACI-318 [24]. The depth of the diagonal strut, a_s , can be taken as the depth of the compression zone of the column, a_c , which can be obtained from the following relationship:

$$a_c = \left(0.25 + 0.85 \frac{N}{A_g f'_c} \right) h_c \quad (3)$$

where h_c is the depth of the column, N is the column axial load, A_g is the gross area of the column cross-section, and f'_c is the cylindrical concrete compressive strength.

Neglecting the contribution of the mid-bars of the columns to the joint shear resistance, the shear strength of specimen TS is estimated using Equation 2. Following the recommendations of ACI 352R [25] for the design of beam-column connections subjected to severe reversal loadings, the ACI-318 building code assumes severe bond deterioration of the reinforcing bars in the joint, and recognizes the diagonal compression strut as the only shear resisting mechanism. Furthermore, depending on the joint geometry and adjoining elements, ACI-318 [24] specifies a minimum amount of joint transverse reinforcement and detailing requirements to ensure an effective joint confinement and to prevent premature buckling of the columns' longitudinal bars. For the joints satisfying these requirements, ACI-318 [24] proposes an empirical relationship, Equation 4, to calculate the joint shear horizontal capacity:

$$V_{jh}^{ACI} = 0.083 \gamma \sqrt{f'_c} A_j \quad (4)$$

where γ is the confinement index that depends on the number and the geometry of the adjoining beams ($\gamma = 12$ for an effectively confined corner joint with upper and lower columns), and A_j is the effective joint area.

In the case of the specimen TSR, the concrete beneath the strengthening scheme was uniformly crushed, thus it can be assumed that the joint was provided with an effective confinement. Therefore, Equation 4 is used to analytically estimate the joint shear strength of this specimen.

The shear strength of TS and TSR, calculated using Equations 2 and 4, respectively, along with the value of the parameters used for their calculations are indicated in Tables 9 and 10, correspondingly. It should be noted that neither of the Equations 2 or 4 takes into account the reduction in the joint shear strength caused by the adverse effects of biaxial loadings. Thus, the calculated joint shear strength by means of Equations 2 or 4, is multiplied in a reduction factor ρ , to take into account this adverse effect. The value of ρ is taken as the maximum degradation in shear strength of the specimen, as reported in Tables 6 and 7.

The comparison of the analytically predicted and the experimentally obtained joint shear strength for the specimen TS indicates that Equation 2 has predicted the joint shear strength

with a negligible underestimation (6% in the last column of Table 9). The corresponding difference in the case of TSR specifies that the ACI-318 relationship, Equation 4, has overestimated the joint shear strength 11% (see the last column in Table 10).

6. CONCLUSIONS

In the present study, seismic shear strengthening of a 3D RC corner beam-column joint using a proposed technique is experimentally investigated. The proposed strengthening scheme is composed of GFRP sheets and a steel cage which was originally designed as an anchorage system for GFRP. According to the obtained results from this study, the following conclusions are drawn:

- (1) Using the proposed technique, noticeable enhancement in both strength and seismic characteristics of the rehabilitated specimen, subjected to the cyclic loading, was obtained. Stiffness, ductility, energy dissipation capacity and the joint shear strength were the main measured enhancements. The brittle joint shear failure mode of the as-built specimen was altered to a ductile one in the strengthened specimen with the plastic-hinges formed at the interface of the beams with the joint.
- (2) The GFRP sheet anchored to the steel cage provided sufficient confinement to the joint concrete that prevented excessive joint shear distortion and maintained the joint integrity at large deformations. Consequently, the storey drift was reduced.
- (3) In contrary to the reference specimen, the degradation in the storey-shear strength of the strengthened specimen, due to the adverse effect of biaxial loadings, was almost negligible.
- (4) Assuming that a cracked diagonal strut was the only shear resisting mechanism, the joint shear strength of the as-built specimen, without joint transverse reinforcement, was well predicted.
- (5) The empirical relationship of ACI-318 for the joint shear strength of those corner beam-column joints detailed with sufficient confining transverse reinforcement in their joint region satisfactorily estimated the joint shear strength of the strengthened specimen. This result along

with the uniformly crushed concrete beneath the GFRP at the joint region indicated the efficiency of the proposed scheme in confining the concrete at the joint region.

(6) The installation of the proposed strengthening technique does not interfere with the existence of the orthogonal beams or the floor slab. Moreover, the technique does not require any perforation on the concrete. These advantages offer practical feasibility in using of this proposed seismic strengthening solution as compared to other investigated techniques.

7. ACKNOWLEDGEMENTS

The experimental part of the study presented in this paper was funded by the International Institute of Earthquake Engineering and Seismology (IEES), project number 7342.

8. REFERENCES

- [1] Engindeniz M, Kahn LF, Zureick A-H. Repair and Strengthening of Reinforced Concrete Beam-Column Joints: State of the Art. *ACI Structural Journal*. 2005;102(2):14.
- [2] Bousselham A. State of Research on Seismic Retrofit of RC Beam-Column Joints with Externally Bonded FRP. *Journal of Composites for Construction*. 2010;14(1):49-61.
- [3] Al-Salloum Y, Almusallam T. Seismic Response of Interior RC Beam-Column Joints Upgraded with FRP Sheets. I: Experimental Study. *Journal of Composites for Construction*. 2007;11(6):575-89.
- [4] Mukherjee A, Joshi M. FRPC reinforced concrete beam-column joints under cyclic excitation. *Composite Structures*. 2005;70(2):185-99.
- [5] Pantelides CP, Okahashi Y, Reaveley LD. Seismic Rehabilitation of RC Frame Interior Beam-Column Joints with FRP Composites. In: *The 14th World Conference on Earthquake Engineering*. Beijing; 2008.
- [6] Karayannis CG, Sirkelis GM. Strengthening and rehabilitation of RC beam-column joints using carbon-FRP jacketing and epoxy resin injection. *Earthquake Engineering & Structural Dynamics*. 2008;37(5):769-90.

- [7] Tsonos AG. Effectiveness of CFRP-jackets and RC-jackets in post-earthquake and pre-earthquake retrofitting of beam-column subassemblages. *Engineering Structures*. 2008;30(3):777-93.
- [8] Danesh F, Esmaceli E, Alam MF. Shear Strengthening of 3D RC Beam-Column Connection Using GFRP: FEM Study. *Asian Journal of Applied Sciences*. 2008;1(3):217-27.
- [9] Ha G-J, Cho C-G, Kang H-W, Feo L. Seismic improvement of RC beam-column joints using hexagonal CFRP bars combined with CFRP sheets. *Composite Structures*. 2013;95(0):464-70.
- [10] Lee WT, Chiou YJ, Shih MH. Reinforced concrete beam-column joint strengthened with carbon fiber reinforced polymer. *Composite Structures*. 2010;92(1):48-60.
- [11] Mahini SS, Ronagh HR. Strength and ductility of FRP web-bonded RC beams for the assessment of retrofitted beam-column joints. *Composite Structures*. 2010;92(6):1325-32.
- [12] Antonopoulos C, Triantafillou T. Experimental Investigation of FRP-Strengthened RC Beam-Column Joints. *Journal of Composites for Construction*. 2003;7(1):39-49.
- [13] Ghobarah A, Said A. Shear strengthening of beam-column joints. *Engineering Structures*. 2002;24(7):881-8.
- [14] Al-Salloum Y, Almusallam T, Alsayed S, Siddiqui N. Seismic Behavior of As-Built, ACI-Complying, and CFRP-Repaired Exterior RC Beam-Column Joints. *Journal of Composites for Construction*. 2011;15(4):522-34.
- [15] Engindeniz M, Kahn LF, Zureick A-H. Pre-1970 RC Corner Beam-Column-Slab Joints: Seismic Adequacy and Upgradability with CFRP Composites. In: *The 14th World Conference on Earthquake Engineering*. Beijing; 2008.
- [16] El-Amoury T, Ghobarah A. Seismic rehabilitation of beam-column joint using GFRP sheets. *Engineering Structures*. 2002;24(11):1397-407.
- [17] Said AM, Nehdi ML. Use of FRP for RC frames in seismic zones: Part I. Evaluation of FRP beam-column joint rehabilitation techniques. *Applied Composite Materials*. 2004;11(4):205-26.

- [18] Parvin A, Altay S, Yalcin C, Kaya O. CFRP Rehabilitation of Concrete Frame Joints with Inadequate Shear and Anchorage Details. *Journal of Composites for Construction*. 2009;14(1):72-82.
- [19] Li B, Kai Q. Seismic Behavior of Reinforced Concrete Interior Beam-Wide Column Joints Repaired Using FRP. *Journal of Composites for Construction*. 2011;15(3):327-38.
- [20] Esmaeeli E. Development of Hybrid Composite Plate (HCP) for the Strengthening and Repair of RC Structures [Doctoral Thesis]. Guimaraes: University of Minho; 2015.
- [21] Kanda T, Watanabe S, Li VC. Application of pseudo strain hardening cementitious composites to shear resistant structural elements. *AEDIFICATIO Publishers, Fracture Mechanics of Concrete Structures*. 1998;3:1477-90.
- [22] Esmaeeli E, Barros JAO, Sena-Cruz J, Varum H, Melo J. Assessment of the efficiency of prefabricated hybrid composite plates (HCPs) for retrofitting of damaged interior RC beam-column joints. *Composite Structures*. 2015;119:24-37.
- [23] Esmaeeli E, Barros JAO, Sena-Cruz J, Fasan L, Li Prizzi FR, Melo J, et al. Retrofitting of interior RC beam-column joints using CFRP strengthened SHCC: Cast-in-place solution. *Composite Structures*. 2015;122:456-67.
- [24] ACI 318-14: Building Code Requirements for Structural Concrete and Commentary: American Concrete Institute (ACI); 2014.
- [25] ACI-ASCE Committee 352. Recommendations for Design of Slab-Column Connections in Monolithic Reinforced Concrete Structures (ACI 352.R-02). ACI; 2002.
- [26] Esmaeeli E. Shear Strengthening of 3D RC Corner Beam-Column Joint using GFRP Layers and Mechanical Anchors [MSc Thesis]. Tehran: K.N. Toosi University of Technology; 2007.
- [27] Standards New Zealand, "NZS 3101:2006, Concrete Structures Standard".
- [28] Hwang S-J, Lee H-J, Liao T-F, Wang K-C, Tsai H-H. Role of Hoops on Shear Strength of Reinforced Concrete Beam-Column Joints. *ACI Structural Journal*. 2005;102(3):445-53.

[29] Hwang S, Lee H. Strength Prediction for Discontinuity Regions by Softened Strut-and-Tie Model. *Journal of Structural Engineering*. 2002;128(12):1519-26.

ACCEPTED MANUSCRIPT

Tables' caption

Table 1: Bidirectional 50/50 glass fabric properties

Table 2: Hardened epoxy resin properties

Table 3: Storey shear capacity of specimen TS

Table 4: Storey-shear at the first yield of longitudinal bars of the beams of specimen TSR

Table 5: Maximum storey-shear capacity of specimen TSR

Table 6: Percentage of reduction in storey shear of horizontal plane due to bidirectional loading cycles without phase difference.

Table 7: Percentage of reduction in the storey shear of horizontal plane due to bidirectional loading cycles with 180° of phase difference.

Table 8: Experimental joint shear strength (under bidirectional loading effect)

Table 9: Joint shear strength of specimen TS based on SST model

Table 10: Joint shear strength of specimen TSR based on ACI-318

Figures' caption

Fig. 1: Geometry of specimens and details of the reinforcement

Fig. 2. Test setup configuration.

Fig. 3. Hollow steel boxes used at each end of the column

Fig. 4. Cyclic loading pattern (the load cycles placed in the dashed-line rectangular shape were repeated by 0.8% increase in their amplitude until 30 percent drop in storey shear capacity occurred; the positive drift-angle corresponds to the push direction and the negative one to the pull direction)

Fig. 5. The layout of the bidirectional glass fabric (dimensions are in mm)

Fig. 6. Rehabilitation scheme (dimensions are in mm).

Fig. 7. Plots of storey-shear *versus* drift-angle of specimen TS in (a) vertical plane, and (b) horizontal plane

Fig. 8. Observed damages in the reference specimen, TS.

Fig. 9. Plots of storey-shear *versus* drift-angle for specimen TSR in (a) vertical plane, and (b) horizontal plane.

Fig. 10. Distribution of the cracks and damages at the end of the test in specimen TSR: (a) flexural cracks distributed along the length of the vertical beam; (b) crushing of concrete beneath the GFRP composite.

Fig. 11. Envelope curve of storey-shear *versus* drift-angle of the reference and the strengthened specimens.

Fig. 12. Contribution of joint shear deformation in storey drift-angle.

Fig. 13. The evolution of the secant stiffness during testing of the specimens

Fig. 14. Cumulative dissipated energy *versus* time and drift-angle (a) up to the ultimate displacement of each specimen, and (b) magnified view of the region enclosed in the rectangle in 14(a). (Note that drift-angle here represents the end of the set of cycles for a given drift-angle).

Fig. 15. Interaction orbits of bidirectional loadings, without phase difference, at 0.8% and 1.6% drift-angles for (a) specimen TS and (b) Specimens TSR

Fig. 16. Interaction orbits of bidirectional loadings, with 180° phase difference, at 1.2% and 2.0% drift-angles for (a) specimen TS and (b) Specimen TSR

Fig. 17. Tensile strains in longitudinal reinforcements of the vertical beam versus the drift-angle, up to the peak load, for (a) specimen TS and (b) specimen TSR

ACCEPTED MANUSCRIPT

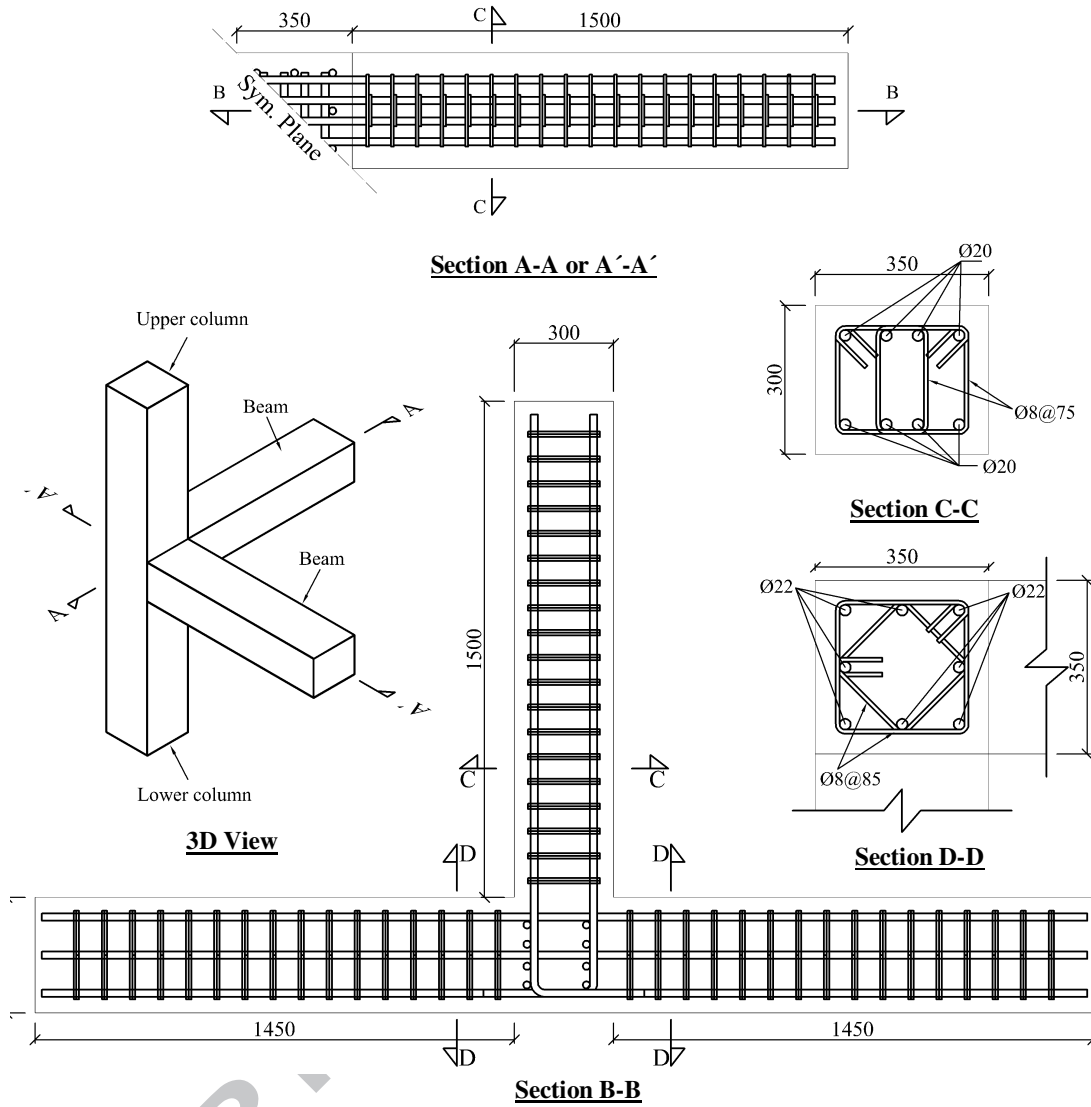


Fig. 1: Geometry of specimens and details of the reinforcement

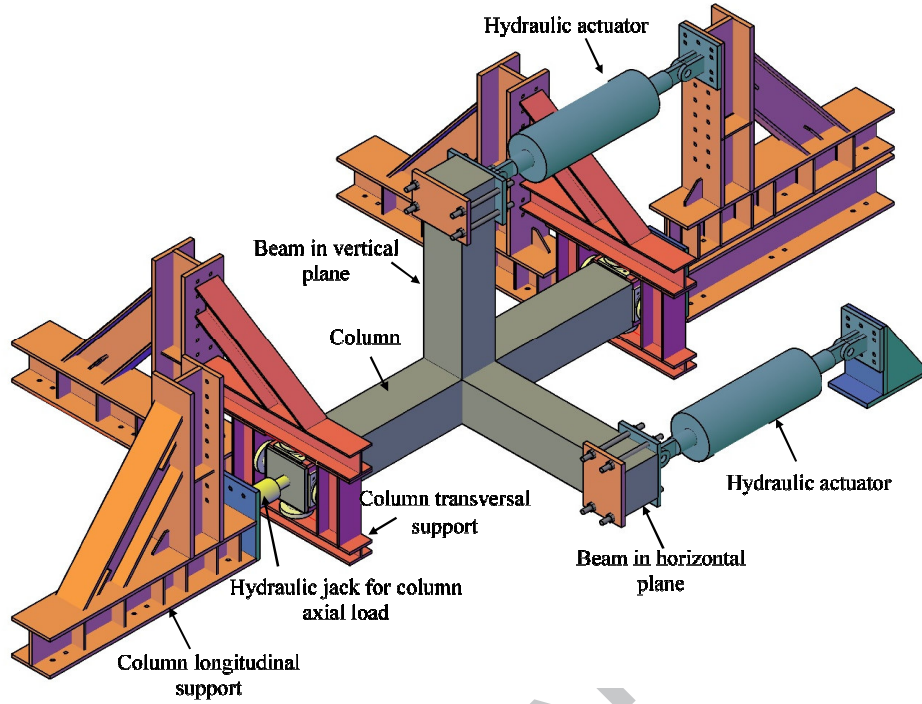


Fig. 2. Test setup configuration.

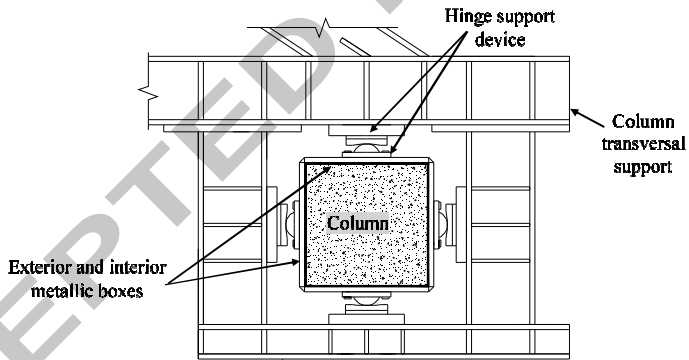


Fig. 3. Hollow steel boxes used at each end of the column

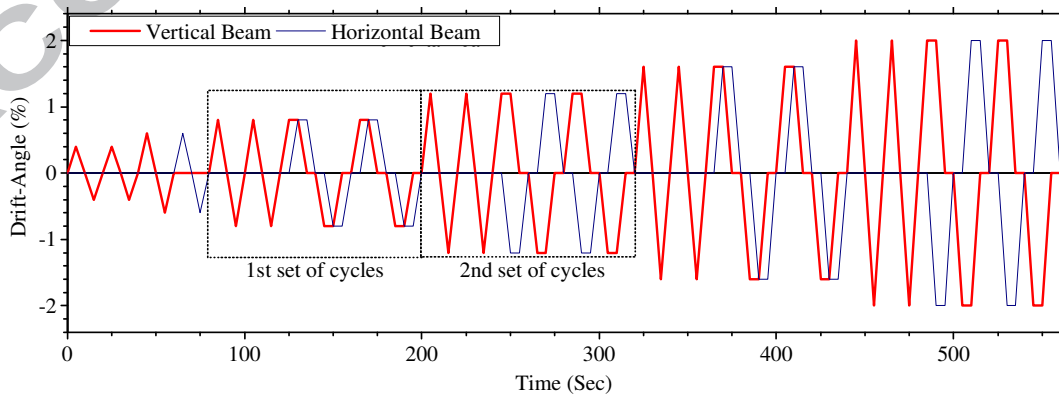


Fig. 4. Cyclic loading pattern (the load cycles placed in the dashed-line rectangular shape were repeated by 0.8% increase in their amplitude until 30 percent drop in storey shear capacity occurred; the positive drift-angle corresponds to the push direction and the negative one to the pull direction)

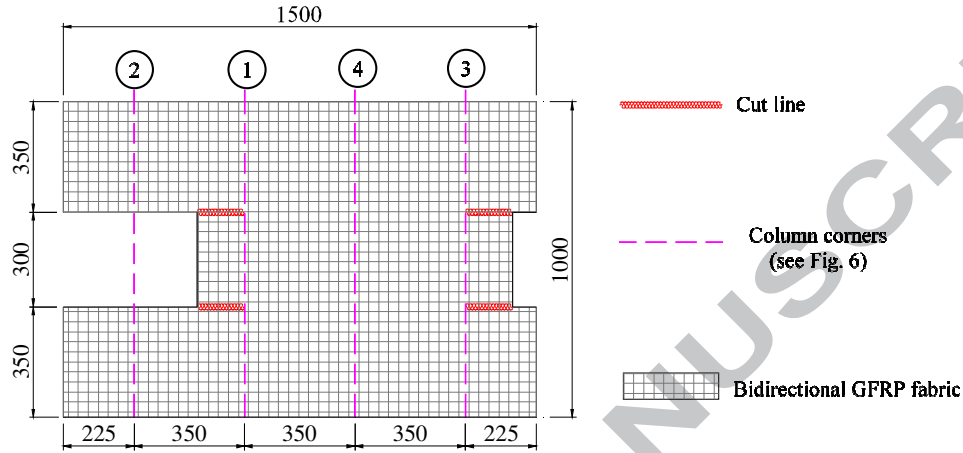


Fig. 5. The layout of the bidirectional glass fabric (dimensions are in mm)

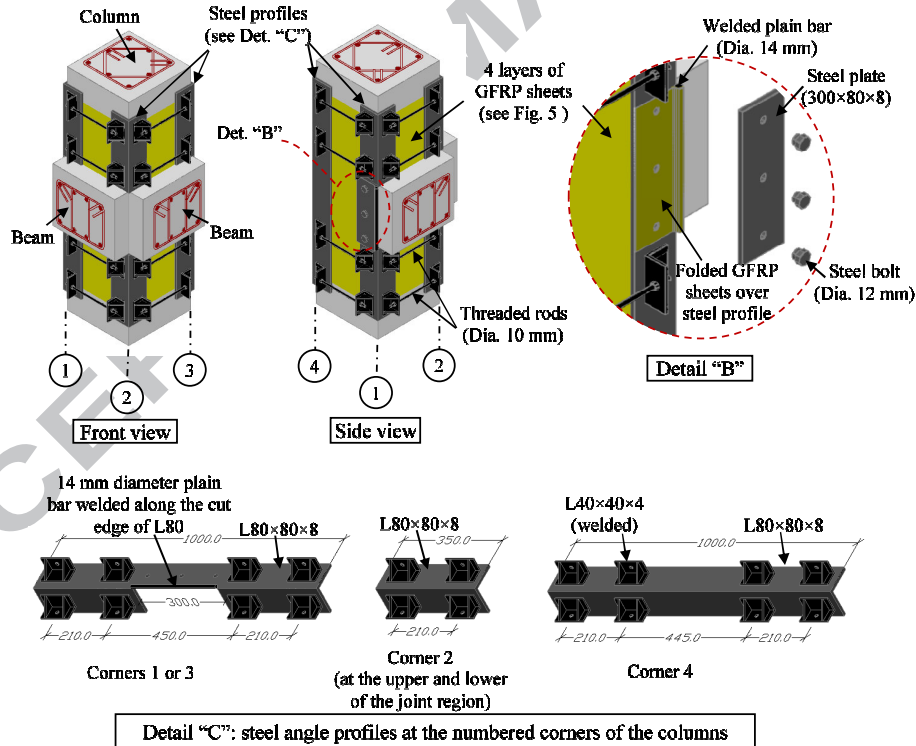


Fig. 6. Rehabilitation scheme (dimensions are in mm).

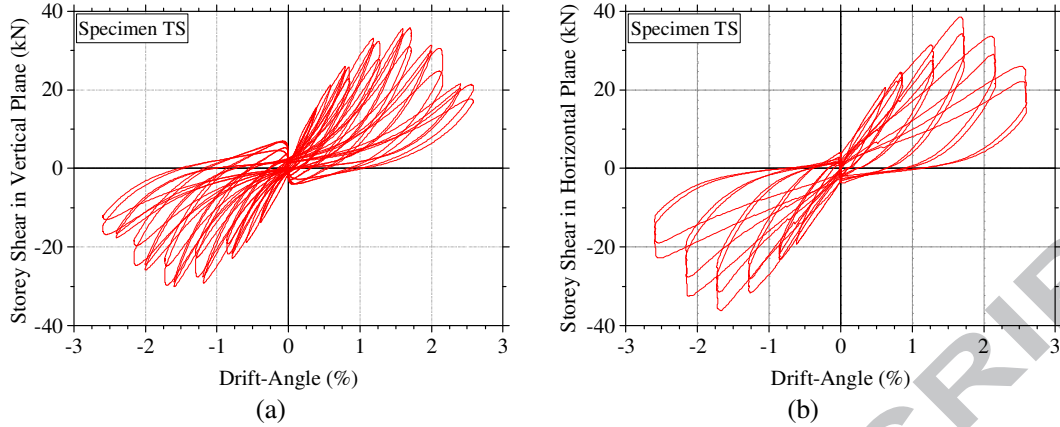


Fig. 7. Plots of storey-shear *versus* drift-angle of specimen TS in (a) vertical plane, and (b) horizontal plane



Fig. 8. Observed damages in the reference specimen, TS.

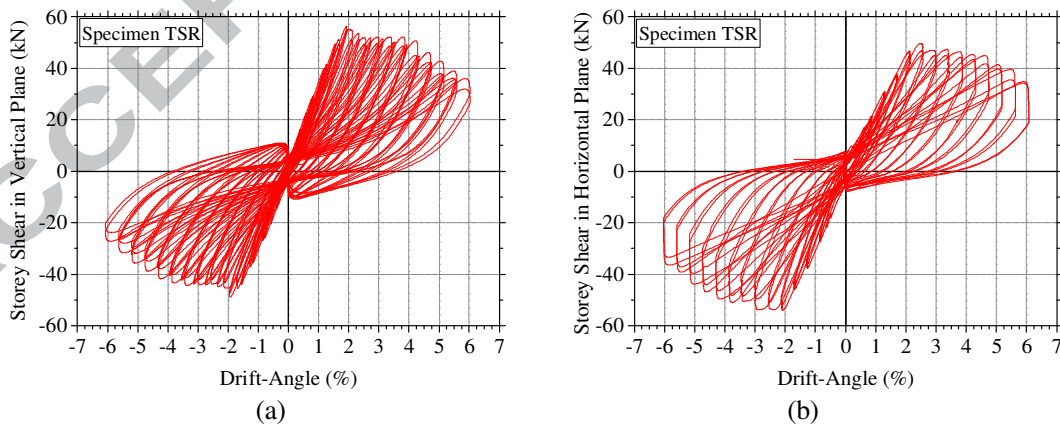


Fig. 9. Plots of storey-shear *versus* drift-angle for specimen TSR in (a) vertical plane, and (b) horizontal plane.

ACCEPTED MANUSCRIPT



Fig. 10. Distribution of the cracks and damages at the end of the test in specimen TSR: (a) flexural cracks distributed along the length of the vertical beam; (b) crushing of concrete beneath the GFRP composite.

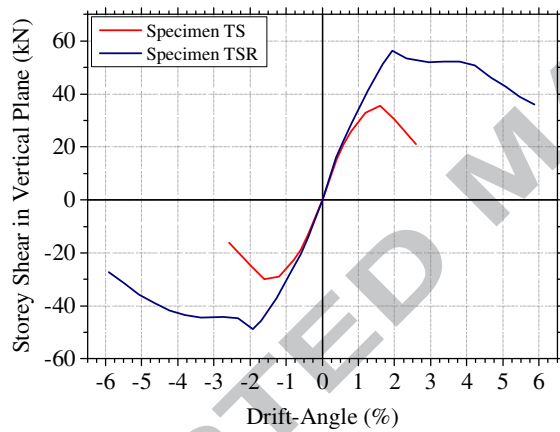


Fig. 11. Envelope curve of storey-shear *versus* drift-angle of the reference and the strengthened specimens, TS and TSR, respectively.

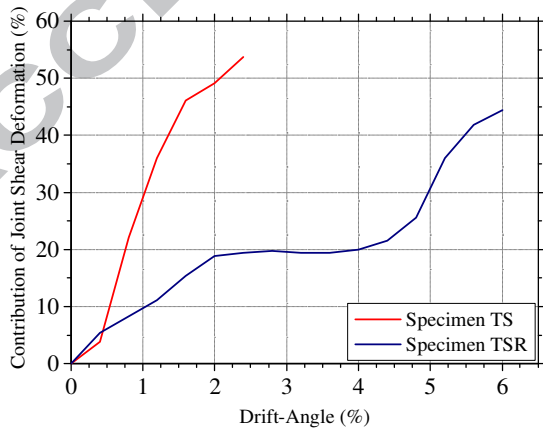


Fig. 12. Contribution of joint shear deformation in storey drift-angle.

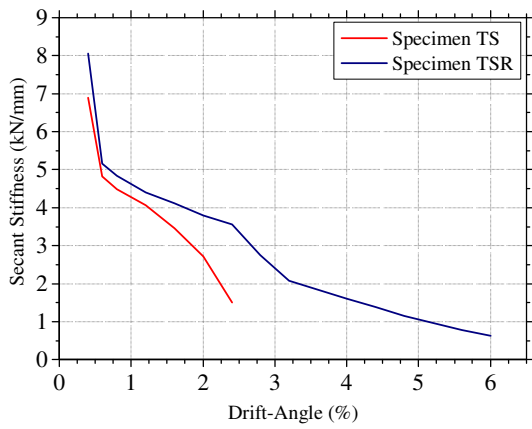


Fig. 13. The evolution of the secant stiffness during testing of the specimens

ACCEPTED MANUSCRIPT

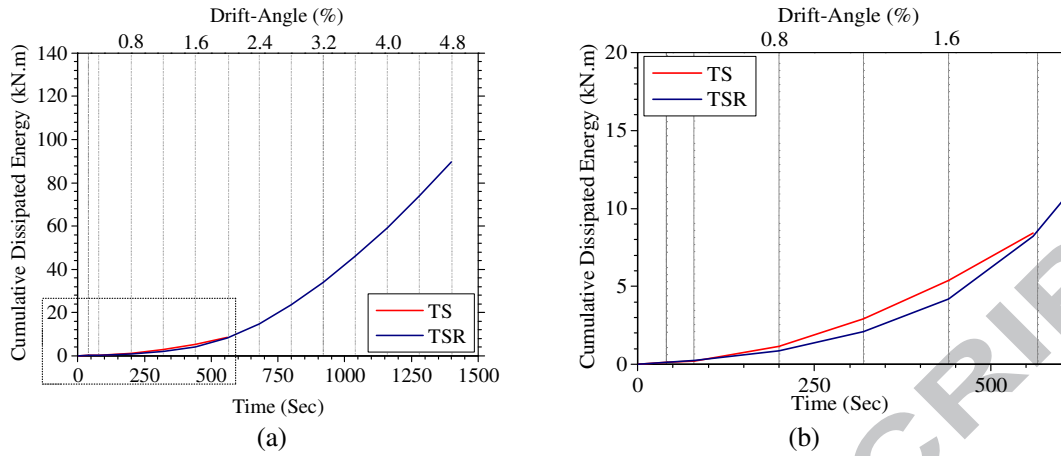


Fig. 14. Cumulative dissipated energy *versus* time and drift-angle (a) up to the ultimate displacement of each specimen and (b) magnified view of the region enclosed in the rectangle in 14(a). (Note that drift-angle here represents the end of the set of cycles for a given drift-angle).

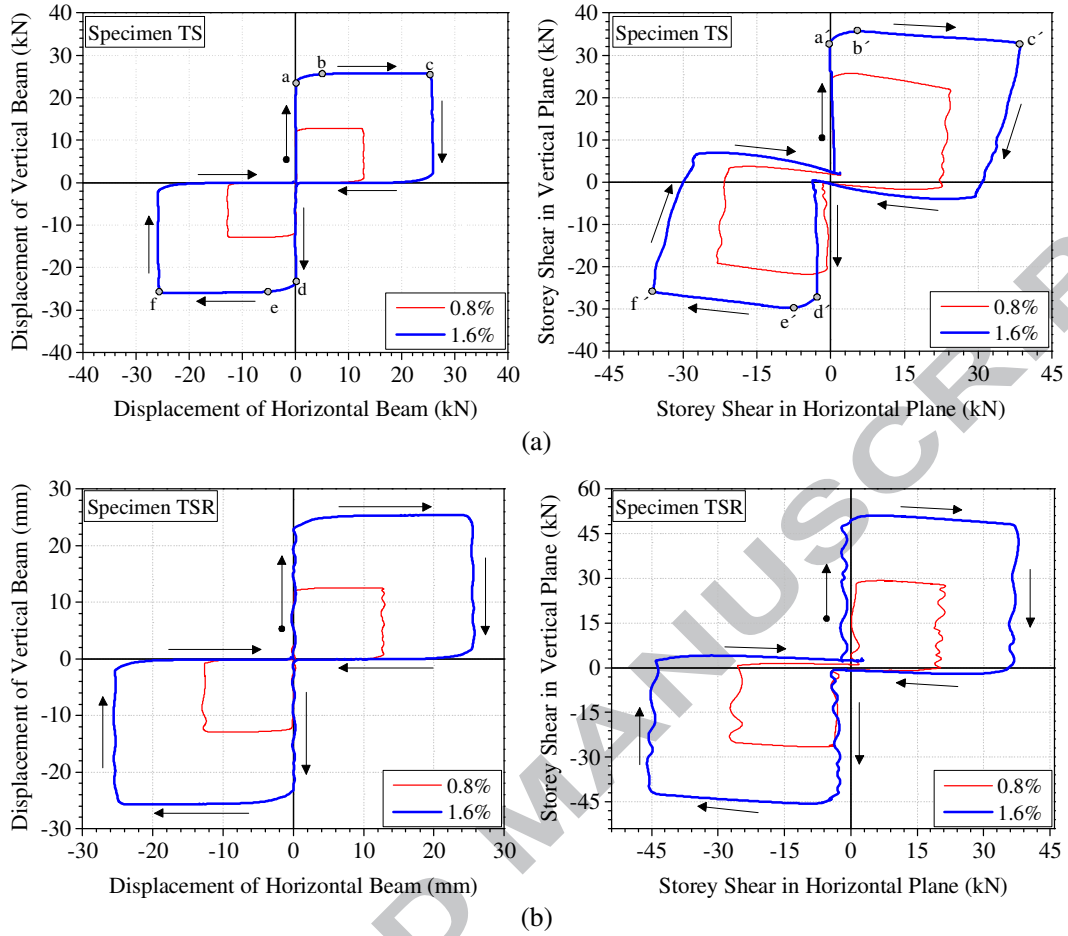


Fig. 15. Interaction orbits of bidirectional loadings, without phase difference, at 0.8% and 1.6% drift-angles for (a) specimen TS and (b) Specimen TSR

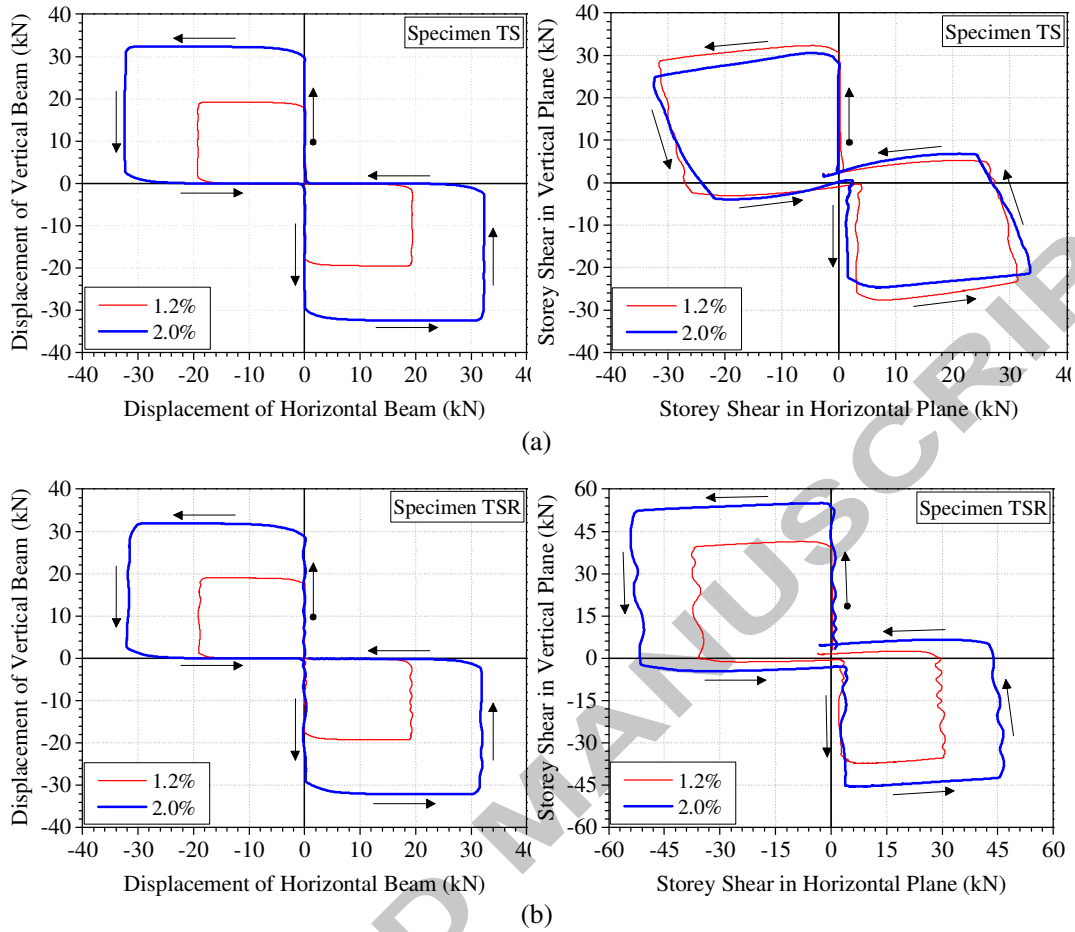
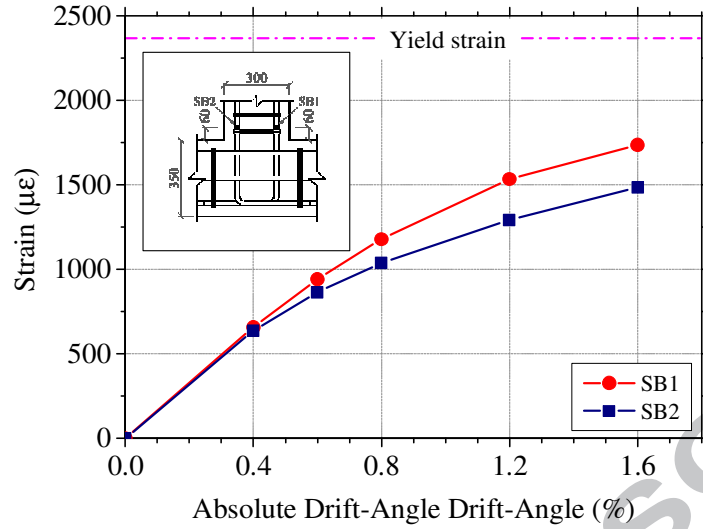
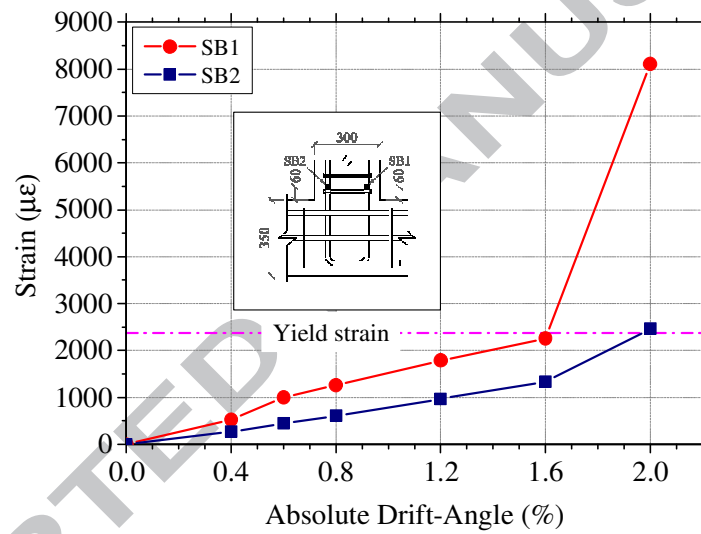


Fig. 16. Interaction orbits of bidirectional loadings, with 180° phase difference, at 1.2% and 2.0% drift-angles for (a) specimen TS and (b) Specimen TSR



(a)



(b)

Fig. 17. Tensile strains in longitudinal reinforcements of the vertical beam *versus* the drift-angle, up to the peak load, for (a) specimen TS and (b) specimen TSR

Table 1: Bidirectional 50/50 glass fabric properties

Tensile strength (MPa)	Modulus of elasticity (MPa)	Design thickness (mm)	Elongation at rupture (%)
3400	73000	0.067	4.5

Table 2: Hardened epoxy resin properties

Tensile strength (MPa)	Modulus of elasticity (MPa)	Compressive strength (MPa)
76.1	2789	97.4

Table 3: Storey shear capacity of specimen TS

	Vertical plane		Horizontal plane	
	Push cycle	Pull cycle	Push cycle	Pull cycle
Peak storey shear (kN)	35.5	30.0	38.6	36.0
Drift angle (%)	1.6	1.6	1.6	1.6

Table 4: Storey-shear at the first yield of longitudinal bars of the beams of specimen TSR

	Vertical plane		Horizontal plane	
	Push cycle	Pull cycle	Push cycle	Pull cycle
Storey-shear (kN)	47.8	48.9	45.7	50.5
Drift angle (%)	1.6	2.0	2.4	2.0

Table 5: Maximum storey-shear capacity of specimen TSR

	Vertical plane		Horizontal plane	
	Push cycle	Pull cycle	Push cycle	Pull cycle
Storey-shear (kN)	56.3	48.9	49.8	54.15
Drift-angle (%)	2.0	2.0	2.4	2.0

Table 6: Percentage of reduction in storey shear of vertical plane due to bidirectional loading cycles without phase difference.

Drift angle	TS			TSR		
	Push	Pull	Avg.	Push	Pull	Avg.
0.8%	15.8%	12.4%	14.1%	5.1%	5.4%	5.3%
1.6%	8.9%	12.7%	10.8%	6.3%	7.1%	6.7%

Table 7: Percentage of reduction in the storey shear of vertical plane due to bidirectional loading cycles with 180° of phase difference.

Drift angle	TS			TSR		
	Push	Pull	Avg.	Push	Pull	Avg.
1.2%	18.7%	13.2%	15.9%	4.9%	6.9%	5.9%
2.0%	11.1%	16.3%	13.7%	4.4%	5.4%	4.9%

Table 8: Experimental joint shear strength (under bidirectional loading effect)

Specimen	ε_{st}^{push} %	ε_{st}^{pull} %	A_{st} mm ²	T_{st}^{push} kN	T_{st}^{pull} kN	V_{col}^{Push} kN	V_{col}^{Pull} kN	V_{jh}^{exp*} kN
TS	0.17	0.15	1257	448.6	395.8	35.5	30.0	389.5
TSR	0.25	0.8		625.8	625.8	56.3	48.9	573.2

* average of push and pull directions

Table 9: Joint shear strength of specimen TS based on SST model

ξ	θ	f'_c	N	A_g	A_{str}	C_d	ρ	V_{jh}^{SST*}	δ^*
-	Degrees	MPa	kN	mm ²	mm ²	kN		kN	%
0.52	45.3	28.7	370	122500	41583	621	0.97	423	-5.9

* $\delta = 100 * (V_{jh}^{SST} - V_{jh}^{exp}) / V_{jh}^{exp}$

Table 10: Joint shear strength of specimen TSR based on ACI-318

f'_c	A_j	γ	ρ	V_{jh}^{ACI*}	δ^*
%	mm ²			kN	%

31.2	122500	12	0.93	635.8	10.9
------	--------	----	------	-------	------

$$* \delta = 100 * (V_{jh}^{ACI} - V_{jh}^{exp}) / V_{jh}^{exp}$$

ACCEPTED MANUSCRIPT